Supporting Information for "Electrical ocean conductivity variability from observations and its budget from an ocean state estimate"

D. S. Trossman,[1,2,3] R. H. Tyler[4,5]

Contents of this file

1. Observations for assessment of ECCOv4r3
2. Observational assessment of ECCOv4r3
3. Temporal variability of OCC and its spatial gradients in ECCOv4r3

---

[1]Earth System Science Interdisciplinary Center, University of Maryland, College Park, MD, USA

[2]Department of Oceanography and Coastal Sciences, Louisiana State University, Baton Rouge, LA, USA

[3]Center for Computation & Technology, Louisiana State University, Baton Rouge, LA, USA

[4]Geodesy and Geophysics Laboratory, Code 61A, NASA Goddard Space Flight Center, Greenbelt, MD, USA

[5]Goddard Earth Science and Technology Research (GESTAR) II, University of Maryland, Baltimore County, MD, USA

4. Multivariate empirical orthogonal function (MEOF) analysis of ECCOv4r3

5. Figures S1-S5

Additional Supporting Information

1. Captions for Figures S1-S5

Observations for assessment of ECCOv4r3

We make use of the optimally interpolated sea surface temperature (OISST) combined with either the Jet Propulsion Laboratory's Soil Moisture Active Passive (SMAP) satellite mission Level-2 sea surface salinity (SSS) or the European Space Agency's Soil Moisture and Ocean Salinity (SMOS) mission Level-2 SSS data sets [*Reul et al.*, 2020] to calculate the sea surface conductivity (SSC). We require the OISST and either SMAP or SMOS data to be within 3.5 days and 50 km of each other to be considered simultaneous. We also mask out regions where the cold brightness temperature biases prevent us from retrieving reliable SSS data. These requirements prevents us from calculating an average or standard deviation of the SSC at every point where there are OISST data.

Because the ECCOv4r3 data are monthly, SMAP samples the same location every eight days, SMOS samples approximately the same location every eight days, and OISST is daily, we averaged the satellite-derived data over monthly time frames to compare its temporal variability with the same from model output. The ECCOv4r3 data have a longer time frame than the SMAP+OISST or SMOS+OISST time frames, so we only used 2010-2015 for ECCOv4r3; using the entire 1992-2015 time period isn't noticeably different. Such a short time frame doesn't allow us to distinguish temporal trends in the data and there are no visually distinguishable differences in the temporal standard deviations of the ECCOv4r3 data over 2010-2015 with

or without detrending. Thus, we only remove the temporal mean (as opposed to trend) when computing the temporal standard deviations in the SSC.

We also make use of the climatological conductivity data described in the Introduction, specifically WOA18 *Reagan et al.* [2019]. The climatology conductivity data is not simply calculated from the temperature and salinity climatology data sets, as in *Manoj et al.* [2006] and *Grayver* [2021]. Rather, to retain thermodynamic consistency and also avoid known observational biases in the differently sampled temperature and salinity observations, the conductivity data is calculated only from co-sampled temperature and salinity observations. To perform a pointwise comparison of the WOA18 product with the ECCOv4r3 product, we calculate a seasonal climatology from the ECCOv4r3 output with the electrical conductivity computed in-line as the model runs and interpolate the WOA18 seasonal climatology data to the LLC90 grid.

Observational assessment of ECCOv4r3

Using the model output of the ECCO re-run, we compare the variability in electrical conductivity with that seen in observations. We first focus on the agreement between satellite-derived data and ECCOv4r3. Figure S1 shows qualitative and generally good quantitative agreement between the satellite-derived sea surface conductivity (SSC) and the ECCOv4r3-calculated surface layer conductivity. The average SSC is highest between 30^oS and 30^oN and lowest at high-latitudes in both the satellite-derived and ECCOv4r3-calculated fields, with their magnitudes very similar (Figs. S1a-c). The temporal standard deviation of SSC is highest in the vicinity of the Gulf Stream and Kuroshio Extension as well as in the Mediterranean Sea, Sea of Japan, and Sea of Okhotsk in ECCOv4r3 (Fig. S1f). These regions are poorly sampled in the satellite data, but to the extent these regions are sampled, the satellite data also find these regions to have

the highest temporal variability (Figs. S1d-e). The satellite-derived data and ECCOv4r3 output agree that the regions with the lowest temporal variability are in both the low- and high-latitude regions (Figs. S1d-f). There is very high correlation between the satellite-derived data and ECCOv4r3 output (> 0.9) everywhere with sufficient satellite sampling.

We turn to assessing the agreement between the WOA seasonal conductivity climatology *Tyler et al.* [2017] and a seasonal climatology constructed from ECCOv4r3 output first presented in *Trossman and Tyler* [2019]. Figure S2 shows that the disagreements between the World Ocean Atlas (2018) and ECCOv4r3 products increase with depth, which is to be expected because of the relative dearth of observations with which ECCO is constrained at deeper depths. Over July-September, the contrast between < 2000 meters depth and > 2000 meters depth is particularly evident in the root-mean-square errors (RMSEs) because summer is the only season when northern high-latitude observations are taken, suggesting the disagreements below 2000 meters depth at northern high-latitudes are larger than elsewhere. The seasonal correlations are high in a globally averaged sense, but are highest (nearly perfect: > 0.98) at shallow depths in the open ocean and go down quickly to about 0.5 or less below about 700 meters depth (not shown). The disagreements are particularly evident at depths approaching 6000 meters depth because of the few constraints, even with ship-based hydrographic data. ECCO achieves relatively small values on continental shelves (particularly where is river outflow) and along some mid-ocean ridges (where geothermal heating is inadequately applied). However, electrical conductivities in ECCO are highly consistent with observations in the vast majority of the ocean.

Temporal variability of OCC and its spatial gradients in ECCOv4r3

We assess the temporal variability in OCC and its horizontal spatial gradients over the entire length of the ECCOv4r3 product (1992-2015). We first remove the averages of the OCC (Fig. S3a), its horizontal spatial gradients (Fig. S3b), and depth-averaged equivalents (Figs. S3c-d), estimated with a best fit via linear regression, before computing the temporal standard deviations of each quantity. The averages of the OCC and its depth-average are very similar to the climatology constructed by *Tyler et al.* [2017] (see their Figure 2). The horizontal spatial gradients in OCC and its depth-average are largest near the coasts and in the Arctic Ocean, with a wealth of fine-scale spatial variability. This is important as these gradients appear in the equations governing ocean electrodynamics. The temporal standard deviations of the linearly detrended OCC (Fig. S4a) are largest in regions with the largest air-sea fluxes. Without detrending, the standard deviations of OCC (not shown) look almost identical to the standard deviations of the sea surface conductivity (Fig. S1f), suggesting that the majority of the variability in OCC occurs near the surface. This is consistent with the findings of *Irrgang et al.* [2018]. The standard deviations of the horizontal gradients in OCC (Fig. S4b) tend to be largest in regions with the steepest topographic slopes as well as in some equatorial regions. The standard deviations of the depth-averaged conductivity (Fig. S4c) are largest on continental shelves and next-largest over mid-ocean ridges because of higher surface variability and their relatively shallow depths, indicating that the seafloor depths primarily determine the spatial pattern. The standard deviations of the horizontal gradients in OCC divided by the seafloor depth h (Fig. S4d) attain their largest values in regions with the largest topographic slopes, demonstrating that their spatial pattern is again primarily set by the seafloor depths. While the near-surface variability clearly plays an important role in setting the variability in OCC and the horizontal gradients in OCC, how the

variability in OCC relates to that in OHC needs to be better understood, which we investigate next.

Multivariate empirical orthogonal function (MEOF) analysis of ECCOv4r3

We apply a multivariate empirical orthogonal function (MEOF) analysis of OCC and OHC to assess their spatial patterns of covariability. We remove the temporal means of the OCC and OHC fields, area-weight each field, and normalize them by their standard deviations prior to calculating the MEOFs, as we did with the EOF analyses shown in Fig. 1. The MEOF analysis suggests the first MEOF (Figs. S5a-b) explains about the same percent of the (co)variance (between one-third and one-half) as our EOF analyses shown in the main text (Figs. 1a-b). The second MEOF for OCC and OHC are related to natural climate variability (Figs. S5c-d) and explains about the same percent of the (co)variance (10-15%) as our EOF analyses shown in the main text (Figs. 1d-e). The MEOF spatial patterns shown in Fig. S5 are visually identical to those shown in Figs. 1a-b and 1d-e, apart from their sign.

References

Grayver, A. V. (2021), Global 3-D electrical conductivity model of the world ocean and marine sediments, *Geochemistry, Geophysics, Geosystems*, **22**, e2021GC009950, https://doi.org/10.1029/2021GC009950

Irrgang, C., J. Saynisch-Wagner, M. Thomas (2018), Depth of origin of ocean-circulation-induced magnetic signals, *Ann. Geophys.*, **36**, 167–180, https://doi.org/10.5194/angeo-36-167-2018

Manoj, C., A. Kuvshinov, S. Maus, H. Luhr, (2006), Ocean circulation generated magnetic signals. *Earth, Planets and Space*, **58**(4), 429–437.

Reagan, J.R., M.M. Zweng, D. Seidov, T.P. Boyer, R.A. Locarnini, A.V. Mishonov, O.K. Baranova, H.E. Garcia, K.W. Weathers, C.R. Paver, I.V. Smolyar, R.H. Tyler (2019). World Ocean Atlas 2018, Volume 6: Conductivity. A. Mishonov Technical Editor, NOAA Atlas NESDIS 86, 38 pp.

Reul, N., S. A. Grodsky, M. Arias, J. Boutin, R. Catany, B. Chapron, F. D'Amico, E. Dinnat, C. Donlon, A. Fore, et al., 2020: Sea surface salinity estimates from spaceborne L-band radiometers: An overview of the first decade of observation (2010–2019). *Remote Sens. Environ.*, **242**, 111769.

Trossman, D. S., R. H. Tyler, 2019: Predictability of Ocean Heat Content from Electrical OCC. *Journal of Geophysical Research-Oceans*, **124**, 667-679; https://doi.org/10.1029/2018JC014740.

Tyler, R. H., T. P. Boyer, T. Minami, M. M. Zweng, J. R. Reagan (2017), Electrical conductivity of the global ocean, *Earth, Planets and Space*, **69**:156, doi:10.1186/s40623-017-0739-7.

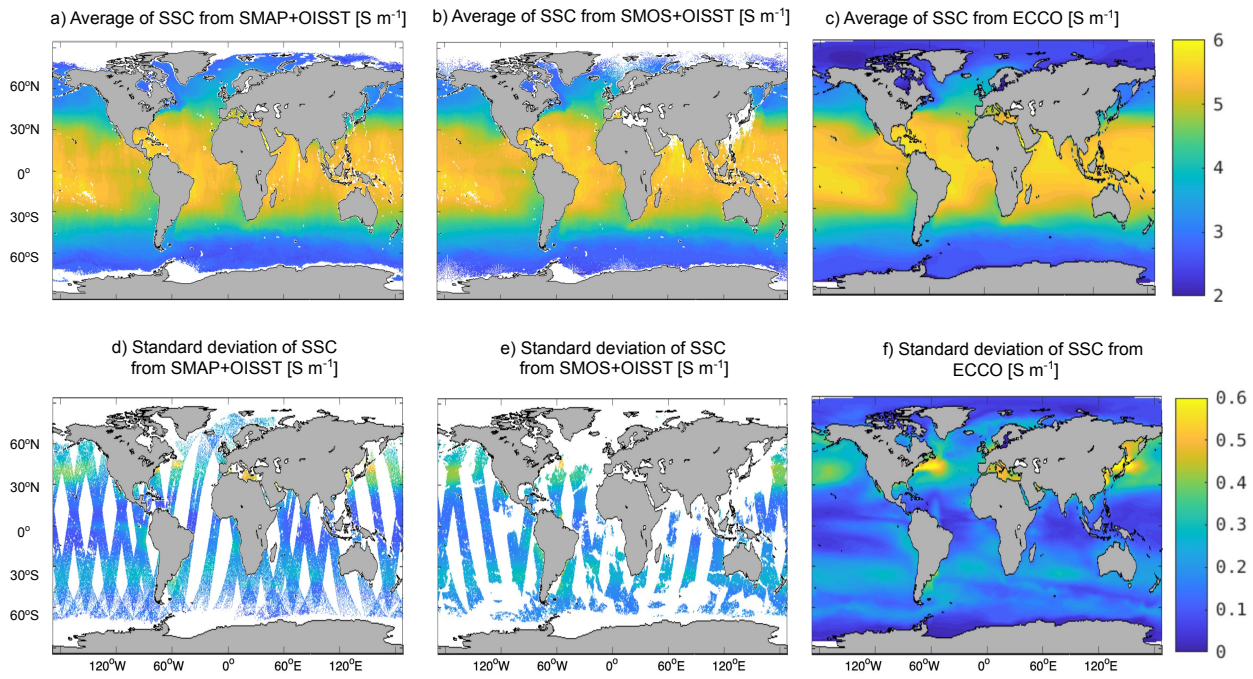

Figure S1. The average sea surface conductivity (SSC [units in S m^{-1}]) (panels a-c) and standard deviation of SSC (panels d-f) over the length of the SMAP mission (April of 2015 through 2021 - panels a and d), over the length of the SMOS mission (June of 2010 through 2021 - panels b and e), and over the length of the ECCOv4r3 product (January of 1992 through 2015 - panels c and f).

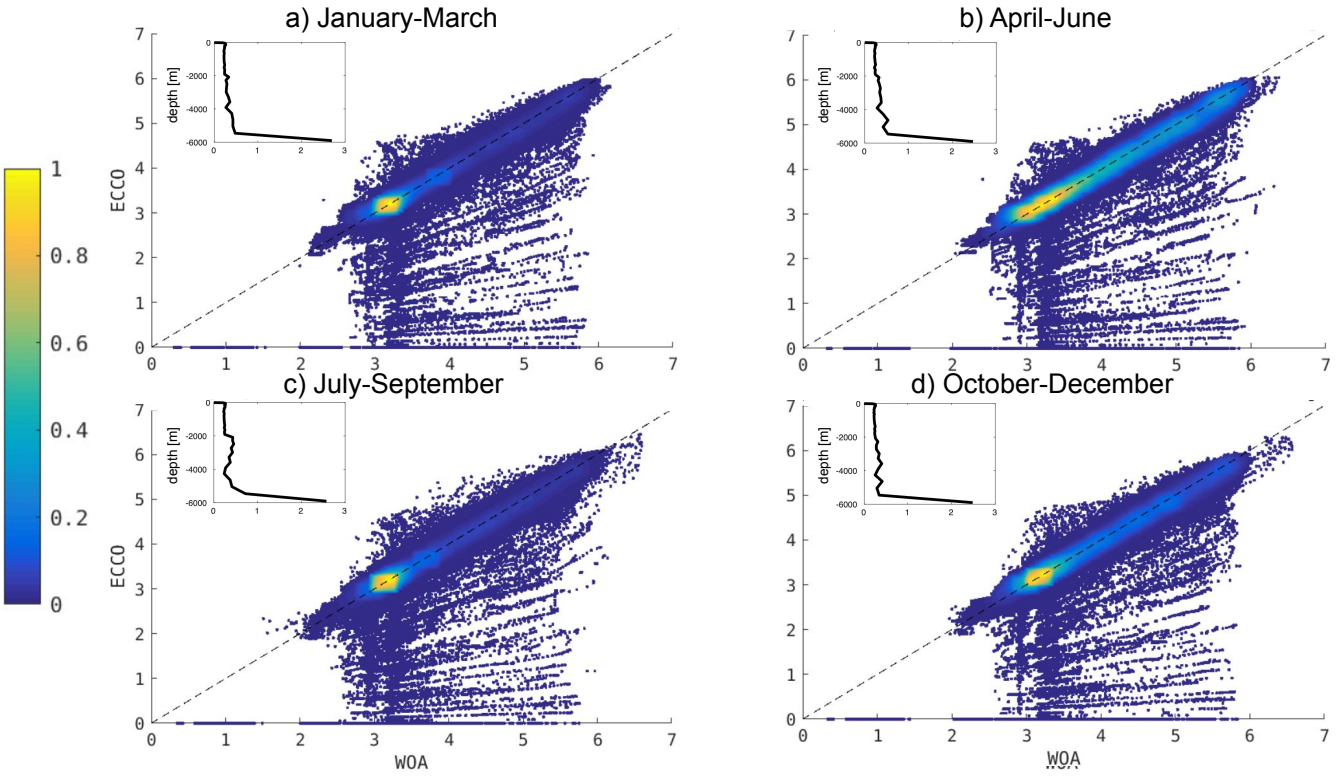

Figure S2. The depth-averaged electrical conductivity from the World Ocean Atlas (2018) or WOA (abscissa) and ECCOv4r3 (ordinate) seasonal climatologies from January-March (panel a), April-June (panel b), July-September (panel c), and October-December (panel d). The inset profiles in each panel indicate the root-mean-square error (RMSE) between the WOA and ECCOv4r3 products as a function of depth.

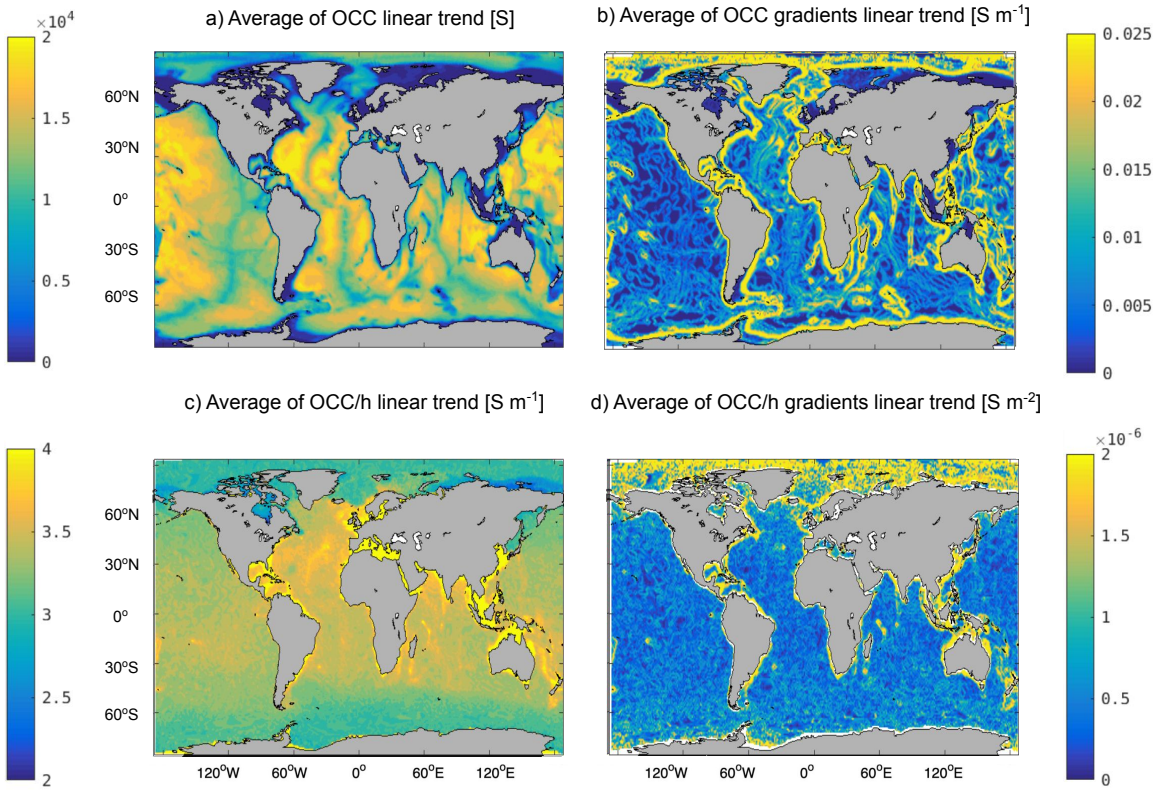

Figure S3. The temporal averages of the linear regression-based predictions for the ocean conductivity content (OCC) (panel a; units in S); horizontal gradients in OCC (b; units in S m^{-1}); depth-averaged electrical conductivity (OCC/h) (c; units in S m^{-1}), and the horizontal gradients in OCC divided by the seafloor depth (d; units in S m^{-2}) from ECCOv4r3.

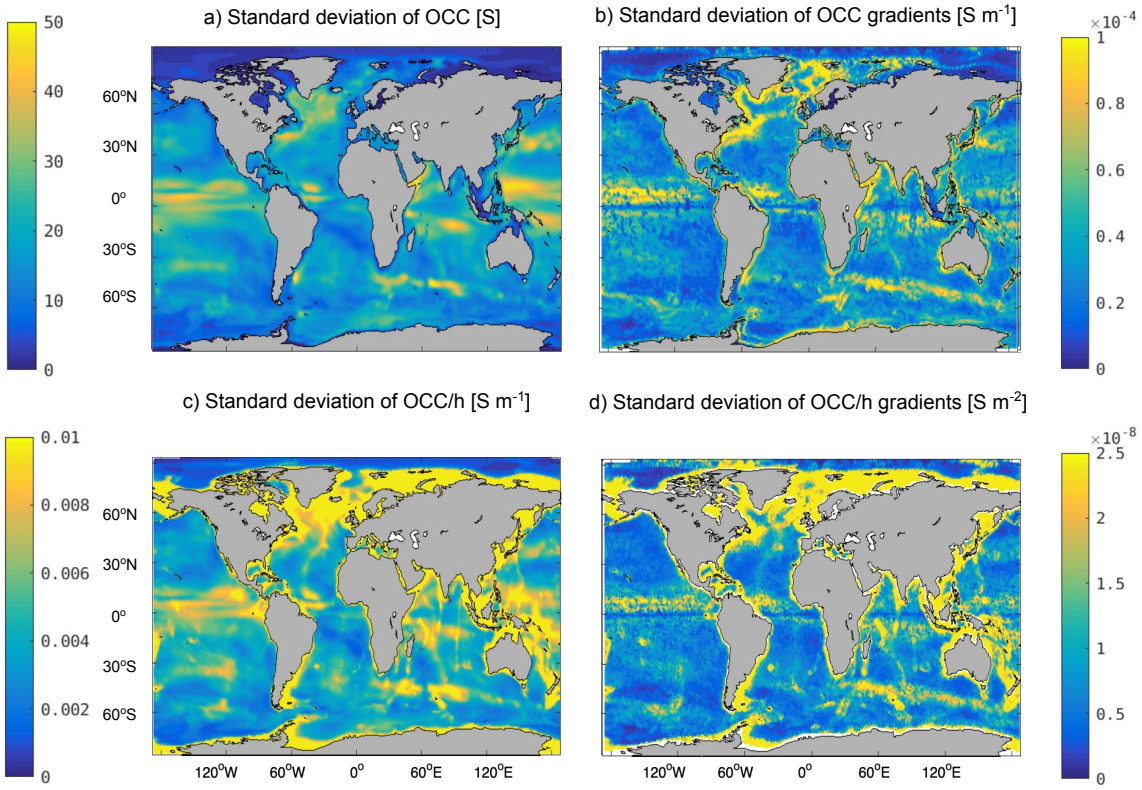

Figure S4. The temporal standard deviations of the ocean conductivity content (OCC) (panel a; units in S); horizontal gradients in OCC (b; units in S m^{-1}); depth-averaged electrical conductivity (OCC/h) (c; units in S m^{-1}), and the horizontal gradients in OCC divided by the seafloor depth (d; units in S m^{-2}) from ECCOv4r3.

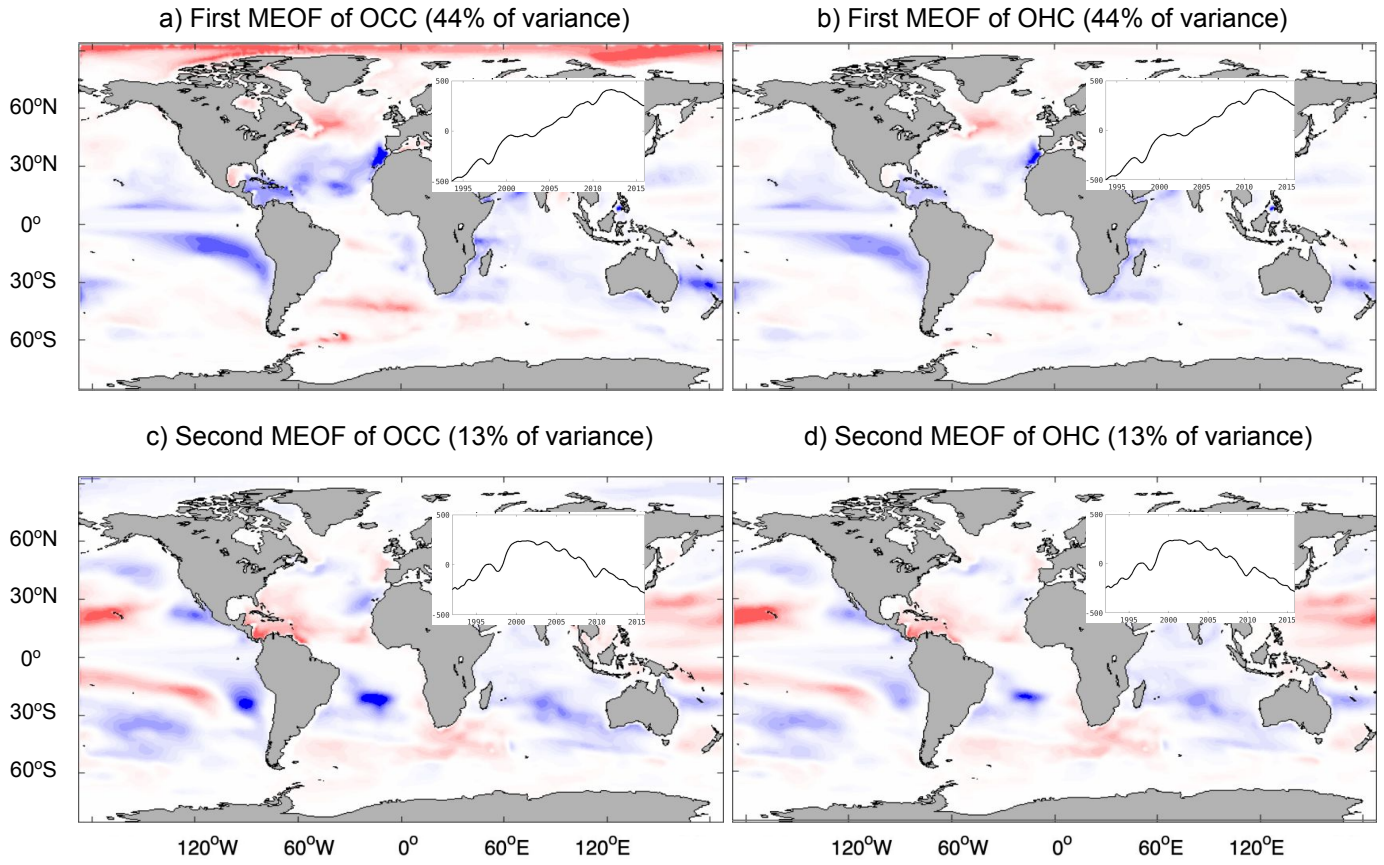

Figure S5. The first (panels a-b) and second (panels c-d) multivariate empirical orthogonal functions for area-weighted and normalized (scaled by standard deviations of) ocean conductivity content (OCC) and ocean heat content (OHC) from ECCOv4r3. The inset time series over Eurasia are the corresponding Principal Components as a function of time. The units are dimensionless for each panel.